ChemComm

The compression of deformed microgels at an air/water interface

Journal:	*ChemComm*
Manuscript ID	CC-COM-07-2023-003425.R2
Article Type:	Communication

Communication

The compression of deformed microgels at an air/water interface

Takahisa Kawamoto,[a] Kohei Yanagi,[a] Yuichiro Nishizawa,[a] Haruka Minato,[a] and Daisuke Suzuki*[ab]

Received 00th January 20xx,
Accepted 00th January 20xx

DOI: 10.1039/x0xx00000x

The compression of deformed hydrogel microspheres (microgels) at air/water interfaces were investigated using a Langmuir-Blodgett trough with simultaneous *in situ* visualization of the process using a fluorescent microscope. The relationship between the structure of the microgel arrays and the compression behavior was clarified using microgels with different degrees of crosslinking.

Hydrogel microspheres (microgels) are soft colloidal particles that contain more than 90% water, and are therefore different from conventional rigid particles made of e.g., polystyrene or silica, in as much as they are highly deformable.[1] Moreover, microgels usually exhibit stimuli-responsiveness, whereby their physicochemical properties can be reversibly changed in response to external stimuli such as changes in temperature and/or pH.[1] Therefore, microgels have found a wide range of applications, in e.g., chemical/biological separation,[2] switchable catalysts,[3] colloidal crystals/glasses,[4] biomedical materials,[5] autonomous actuators,[6] and particulate stabilizers.[7]

Furthermore, it is widely accepted that soft microgels demonstrate unique behavior at fluid interfaces, i.e., at air/water[8] and oil/water interfaces.[9] For instance, microgels composed of poly(*N*-isopropyl acrylamide) (pNIPAm),[1,10] a typical thermoresponsive polymer, show surface activity, undergo a large deformation within a short period of time when adsorbed at an air/water interface.[11] To date, a considerable amount of research has been dedicated to understanding phenomena related to the deformation of microgels at fluid interfaces.[11,12] In our group, we have investigated the drying behavior of sessile droplets that contain various soft particles, including microgels,[13] and found that deformed microgels at the air/water interface become more regularly arranged over time, whereby the center-to-center distances of the microgels decrease.[11b,13c] This process results in the compression of the deformed microgels at the air/water interfaces, and thus the microgels are further deformed at the interface as the surface area of the sessile droplets decreases. To the best of our knowledge, in most studies on microgels at fluid interfaces (i.e., compression studies of microgel arrays at fluid interfaces using a Langmuir-Blodgett (LB) trough[14]), the structure of the microgel arrays is visualized and analyzed after transferring them onto solid substrates. However, this transfer may lead to structural changes of microgel arrays since the structures of microgel arrays are not always the same at fluid interfaces as they are on solid substrates.[13c,14d,15] Therefore, one could argue that the compression of deformed microgels at fluid interfaces has not yet been fully understood.

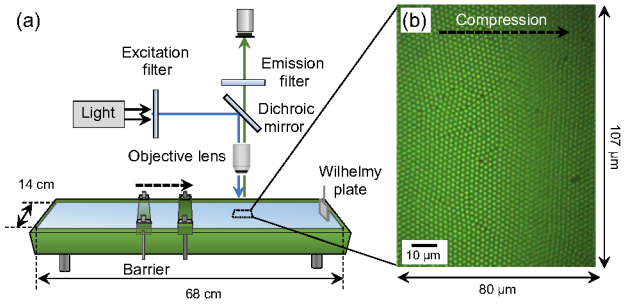

Fig. 1. (a) Schematic illustration of the Langmuir-Blodgett system equipped with a fluorescent microscope for visualizing the air/water interface, where the total area is 952 cm^2 (14 cm × 68 cm) used in this study. (b) Typical fluorescent microscope images of microgels adsorbed at the air/water interface at π = 5 mN/m, where the visible area is 8560 μm^2.

Herein, we demonstrate that direct visualization of microgel arrays adsorbed at an air/water interface is crucial to clarify the relationship between the structure of the microgel array and the π-*A* isotherms acquired from the LB technique. In this study, we assemble a LB trough equipped with a fluorescence microscope, which enabled us to simultaneously determine the structure of microgel arrays at fluid interfaces and the π-A isotherm (Fig. 1a). As shown in Fig. 1b and Movie S1, via fluorescence-microscopy observations, real-time movies of microgel arrays adsorbed at interfaces can be obtained (visible area: 8560 μm^2).

Herein, microgels are labeled chemically with a fluorescent dye using carbodiimide chemistry, which allow visualizing individual microgels clearly adsorbed at the interface (Fig. 1b). First, poly(NIPAm-*co*-fumaric acid) microgels with different

[a] *Graduate School of Textile Science & Technology, Shinshu University, 3-15-1 Tokida, Ueda, Nagano 386-8567, Japan.*
[b] *Research Initiative for Supra-Materials, Interdisciplinary Cluster for Cutting Edge Research, Shinshu University, 3-15-1 Tokida, Ueda, Nagano 386-8567, Japan. d_suzuki@shinshu-u.ac.jp.*
Electronic Supplementary Information (ESI) available: [details of any supplementary information available should be included here]. See DOI: 10.1039/x0xx00000x

amounts of a crosslinker, *N*,*N*'-methylenebis(acrylamide) (BIS), were synthesized via aqueous free radical precipitation polymerization.[1] Fumaric acid was selected as it has carboxy groups capable of chemically binding a fluorescent dye, which was in this case fluorescein. The obtained microgels were uniform in size, as confirmed using optical microscopy (Fig. S1). The size of these microgels in water was ca. 1 μm, which was determined from the optical-microscopy images obtained where the apparent volume fraction ϕ_{eff} was equal to 1 ($D_{\phi eff = 1}$) and the microgels form colloidal crystals (Table S1).[16] From phase images taken using atomic-force microscopy (AFM), it was confirmed that uniformly sized microgels with different structures were formed with different degrees of crosslinking (Fig. 2 and Fig. S2). The microgels were confirmed to have highly deformable core-shell (CS) structures, especially when the quantity of BIS fed during the polymerization was low (Fig. 2). In contrast, the deformation of the microgels was suppressed and the shells were barely visible when the amount of fed BIS during the polymerization was increased (Fig. S2). This result is consistent with a previous report on pNIPAm-based microgels prepared via precipitation polymerization.[10b,17] Hereafter, each microgel is denoted as CS*X*, i.e., CS0.60, CS0.68, CS0.80, and CS0.88, where *X* denominates the core-shell ratio, i.e., the diameter of core (D_{core}) divided by that of the core-shell ($D_{core\text{-}shell}$) as measured from the AFM phase images of the isolated microgels (Table S1 and Fig. S2). D_{core} and $D_{core\text{-}shell}$ were obtained by measuring the diameters of each white circle in the phase images.

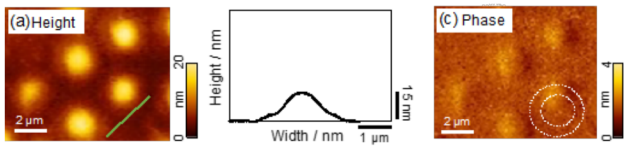

Fig. 2. (a) AFM height image, (b) cross-sectional profile constructed from the green line in the height image (a), and (c) phase image of the CS0.60 microgel deformed on a glass substrate. The two white circles of different sizes in the AFM phase image indicate the core and the core-shell of a microgel (D_{core} = 1676 nm, N = 5; $D_{core\text{-}shell}$ = 2808 nm, N = 3).

Next, to investigate how the microgels are compressed at the air/water interface, the interfacial behavior of microgels adsorbed at the interface was monitored using an LB trough equipped with a fluorescence microscope (Fig. 1a). As shown in Fig.3, the fluorescence-microscopy images (Fig. 3a-f) and their fast-Fourier-transform (FFT) (Fig. 3g-l) analysis showed that the least crosslinked microgels (CS0.60) arrange in an ordered hexagonal structure in most areas of the interface upon increasing the surface pressure, π, i.e., at 1 mN/m (Fig. S3). At π = 1 mN/m, the nearest neighbor distance, D_{NND}, between the CS0.60 microgels was larger than $D_{\phi eff=1}$ in a three-dimensionally packed state, but smaller than $D_{core\text{-}shell}$ in an isolated state on a solid substrate (CS0.60 microgel; $D_{\phi eff = 1}$ = 1650 nm < $D_{NND,\pi = 1}$ = 2223 nm < $D_{core\text{-}shell}$ = 2808 nm). This finding suggests that the microgels were deformed and loosely compressed at the air/water interface, even at a low value of π. It should also be noted here that the individual microgels could not be monitored at ~0 mN/m due to the rapid movement of the microgels, even with the barrier stopped. Subsequently, the D_{NND} gradually decreased during compression whilst maintaining the hexagonal structure, which was confirmed by FFT analysis (Fig. 3 and Fig. S4; e.g., D_{NND} = 2149 nm at 5 mN/m, 2067 nm at 10 mN/m, 1995 nm at 15 mN/m, 1902 nm at 20 mN/m, and 1598 nm at 25 mN/m). The ordered hexagonal structure was maintained as long as the compressed microgels could be individually visualized using fluorescence microscopy (Fig. 3f and Fig. S5). To examine the effect of nanostructures of the microgels on their arrays at the air/water interface during compression, microgels with higher crosslinking densities and smaller shell thicknesses, i.e., CS0.68, CS0.80, and CS0.88 were also evaluated (Figs. S6-S8). We confirmed that, similar to the CS0.60 microgels, these microgels also form hexagonal structures at the air/water interface regardless of the degree of compression.

Here, in order to clarify the importance of visualizing the microgel arrays at the air/water interface, the ordered structures of the microgels on glass substrates were also examined, once the microgel arrays had been transferred from the air/water interface at a certain π (Fig. S9). The microgel arrays on glass substrates also exhibited hexagonal structures at lower π (5 and 10 mN/m). In contrast, for the highly crosslinked CS0.80 and CS0.88 microgels, the microgel arrays formed at the air/water interface were disordered once they had been transferred onto the substrates, and clusters of dense hexagonal structures of microgels were obtained at higher π (e.g., π = 15 and 20 mN/m for CS0.88 and 25 mN/m for CS0.80 and CS0.88). We have already reported that the ordered structure of microgels adsorbed at the air/water interface of a sessile droplet differs from that on a substrate after drying (removal of water), which is mainly due to the decrease of interpenetration

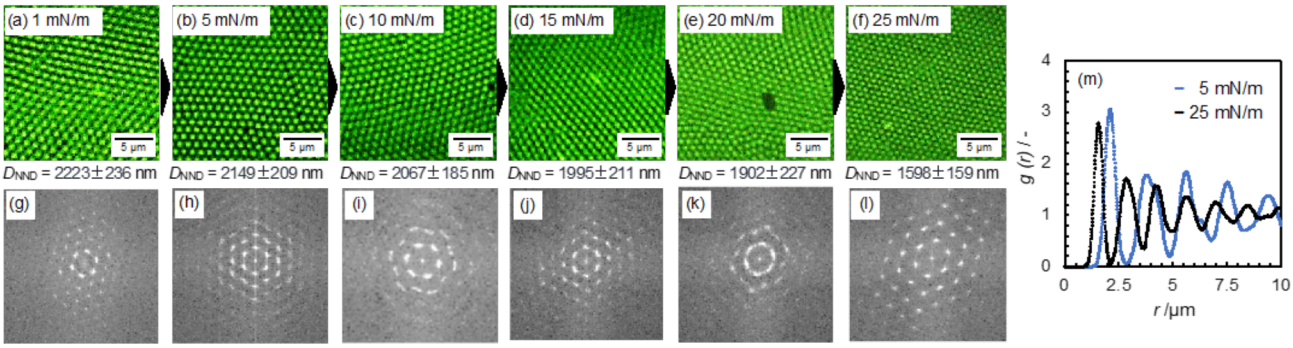

Fig. 3. (a)-(f) Fluorescence microscopy images and (g)-(l) fast-Fourier-transform (FFT) images of the CS0.60 microgels adsorbed at the air/water interface during compression. (m) The pair-correlation function of the microgel arrays calculated from the fluorescence microscopy images taken at 5 and 25mN/m.

between neighboring microgels at the air/water interface.[13cdf,15] Thus, in this study, the lower crosslinked CS0.60 and CS0.66 microgels with thicker shell layers promote interpenetration with each other and prevent microgel arrays from disordering. Moreover, it was clarified that the disordering of microgel arrays is also related to the degree of compression when transferring them to solid substrates. Taking these results into account, it is obvious that direct visualization of the fluid interface is of great importance in order to discuss the relationships between the structures of microgels arrays and their properties and functions.

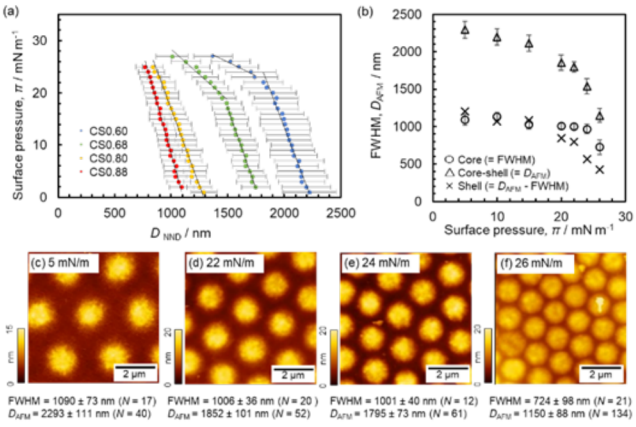

Fig. 4. (a) Correlation between the nearest-neighbor distances, D_{NND}, which were calculated from fluorescence microscopy images of the microgels at the air/water interface, and the surface pressure, π. (b) Diameters of core (= full width at half maximum, FWHM), core-shell (= D_{AFM}), and shell (= D_{AFM} – FWHM) of the CS0.60 microgels transferred onto solid substrates as a function of π. These diameters were evaluated based on AFM height images at (c) 5 mN/m, (d) 22 mN/m, (e) 24 mN/m, and (f) 26 mN/m.

In order to understand the compression process in more detail, the correlation of D_{NND} and π was analyzed based on the visualization of the microgel arrays at the air/water interface (Figs. S4, S6-S8, S10). A two-step plot was observed for the CS0.60 and CS0.68 microgels, whilst a linear one-step slope was obtained for the CS0.80 and CS0.88 microgels (Fig. 4a), indicating that the impact of compression on the microgel deformation differs significantly depending on the microgel structure. Here, to clarify the reason for this different behavior, microgel arrays were transferred onto solid substrate in order to visually examine them by AFM (Fig.4c-f, Fig.S11). It should be noted here that, as has been explained above, structures of microgel arrays of CS0.60 were not disrupted after the transfer. Here, the full width at half maximum (FWHM) as core diameter, the center-to-center distance (D_{AFM}), and shell length (= D_{AFM} - FWHM) of CS0.60 microgel arrays were measured (Fig. 4b and Fig. S11). Based on Fig. 4b, it is clear that D_{AFM}, FWHM, and the shell length decreased with increasing π. During the first stage, both FWHM and the shell length decrease monotonously. Then, during the second stage, the decrease in shell length predominates ($22 \leq \pi \leq 26$ mN/m). In particular, at $\pi = 26$ mN/m, the shell length almost disappears, and the shape of each core changes from spherical to hexagonal (Fig. 4f), accompanied by a marked decrease in D_{AFM} (Fig. 4b). These results indicate that core and shell are compressed for each individual CS0.60 microgel in the microgel arrays during the first stage ($\pi \leq 20$ mN/m), before shell compression becomes dominant during the second stage ($22 \leq \pi \leq 26$ mN/m), where the shape change in each individual CS0.60 microgel was confirmed after the thin shell disappeared. Although the relationship between D_{NND} and π was not clear at that point (Fig.4a), given that a visualization of the microgel arrays at the air/water interface above 27 mN/m for CS0.60 (Fig. S5) was not possible, the decrease in core diameter (~FWHM) seems to be dominant above 27 mN/m. Thus, further investigations into the compression of microgel arrays at interfaces using lager microgels in the wider range of π are indispensable. Nevertheless, our results obtained within the confines of this study represent an important first step to visualize and analyze microgel arrays *in situ*. A deeper understanding of structural changes in microgel arrays at interfaces during compression can be expected to be beneficial, especially where microgels play a crucial role as particulate stabilizers.

In conclusion, the compression behavior of soft microgels adsorbed at air/water interfaces was visualized and quantified for the first time using a Langmuir-Blodgett (LB) system equipped with a fluorescence microscope. The deformed microgels adopt ordered hexagonal structures at the air/water interface and these ordered structures are maintained during compression regardless of the degree of crosslinking density of the microgels. Moreover, the compression behavior was affected by the core-shell ratio of each microgel, whereby the deformation of low-density shells is dominant during the later stage of surface compression. Our findings provide new insights into where surface compression for microgels is crucial, including emulsions and foams stabilized by microgels.

D.S. gratefully acknowledges a CREST grant-in-aid (JPMJCR21L2) from the Japan Science and Technology Agency (JST). H.M. gratefully acknowledges a Grant-in-Aid for Scientific Research (C) (22K05208) from the Japan Society for the Promotion of Science (JSPS).

Conflicts of interest

There are no conflicts to declare.

Notes and references

1 (a) R. Pelton, *Adv Colloid Interface Sci.*, 2000, **85**, 1–33; (b) S. Nayak, L. A. Lyon, *Angew. Chem., Int. Ed.*, 2005, **44**, 7686–7708; (c) F. A. Plamper, W. Richtering, *Acc. Chem. Res.*, 2017, **50**, 131–140; (d) D. Suzuki, K. Horigome, T. Kureha, S. Matsui, T. Watanabe, *Polym. J.*, 2017, **49**, 695–702; (e) M. Karg, A. Pich, T. Hellweg, T. Hoare, L. A. Lyon, J. J. Crassous, D. Suzuki, R. A. Gumerov, S. Schneider, I. I. Potemkin, W. Richtering, *Langmuir*, 2019, **35**, 6231–6255; (f) Y. Nishizawa, K. Honda, D. Suzuki, *Chem. Lett.*, 2021, **50**, 1226–1235.

2 (a) Y. Hoshino, K. Imamura, M. Yue, G. Inoue, Y. Miura, *J. Am. Chem. Soc.*, 2012, **134**, 18177–18180; (b) H. Kawaguchi, *Polym. Int.*, 2014, **63**, 925–932; (c) T. Kureha, Y. Nishizawa, D. Suzuki, *ACS Omega*, 2017, **2**, 7686–7694; (d) T. Kureha, D. Suzuki, *Langmuir*, 2018, **34**, 837–846; (e) S. Matsui, K. Hosho, H. Minato, T. Uchihashi, D. Suzuki, *Chem. Commun.*, 2019, **55**,

10064–10067; (f) C. C. Cutright, J. L. Harris, S. Ramesh, S. A. Khan, J. Genzer, S. Menegatti, *Adv. Funct. Mater*., 2021, **31**, 2104164.

3 (a) M. Ballauff, Y. Lu, *Polymer*, 2007, **48**, 1815–1823; (b) S. Wu, J. Dzubiella, J. Kaiser, M. Drechsler, X. Guo, M. Ballauff, Y. Lu, *Angew. Chem., Int. Ed.*, 2012, **51**, 2229–2233; (c) T. Kureha, Y. Nagase, D. Suzuki, *ACS Omega*, 2018, **3**, 6158–6165; (d) V. Sabadasch, M. Dirksen, P. Fandrich, J. Cremer, N. Biere, D. Anselmetti, T. Hellweg, *ACS Appl. Mate*r. *Interfaces* 2022, **14**, 49181–49188; (e) T. Kharandiuk, K. H. Tan, I. Kubiska, M. A. A. Enezy-Ulbrich, V. Ivasiv, R. Nebesnyi, I. I. Potemkin, A. Pich, *React. Chem. Eng.* 2022, **7**, 2192–2201.

4 (a) T. Hellweg, C. D. Dewhurst, E. Bruckner, K. Kratz, W. Eimer, *Colloid Polym. Sci*., 2000, **278**, 972–978; (b) L. A. Lyon, J. D. Debord, S. B. Debord, C. D. Jones, J. G. McGrath, M. J. Serpe, *J. Phys. Chem. B*, 2004, **108**, 19099–19108; (c) D. Suzuki, J. G. McGrath, H. Kawaguchi, L. A. Lyon, *J. Phys. Chem. C*, 2007, **111**, 5667–5672; (d) J. Mattsson, H. M. Wyss, A. Fernandez-Nieves, K. Miyazaki, Z. Hu, D. R. Reichman, D. A. Weitz, *Nature*, 2009, **462**, 83–86; (e) D. Suzuki, T. Yamagata, K. Horigome, K. Shibata, A. Tsuchida, T. Okubo, *Colloid Polym. Sci.*, 2012, **290**, 107–117; (f) S. Minami, D. Suzuki, K. Urayama, *Curr. Opin. Colloid Interface Sci.*, 2019, **43**, 113–124.

5 (a) S. Saxena, C. E. Hansen, L. A. Lyon, *Acc. Chem. Res.*, 2014, **47**, 2426–2434; (b) A. C. Brown, S. E. Stabenfeldt, B. Ahn, R. T. Hannan, K. S. Dhada, E. S. Herman, V. Stefanelli, N. Guzzetta, A. Alexeev, W. A. Lam, L. A. Lyon, T. H. Barker, *Nat. Mater*., 2014, **13**, 1108–1114; (c) M. Nakamoto, T. Nonaka, K. J. Shea, Y. Miura, Y. Hoshino, *J. Am. Chem. Soc.*, 2016, **138**, 4282–4285.

6 (a) D. Suzuki, T. Sakai, R. Yoshida, *Angew. Chem., Int. Ed*., 2008, **47**, 917–920; (b) D. Suzuki, H. Taniguchi, R. Yoshida, *J. Am. Chem. Soc.*, 2009, **131**, 12058–12059; (c) D. Suzuki, T. Kobayashi, R. Yoshida, T. Hirai, *Soft Matter*, 2012, **8**, 11447–11449; (d) S. Matsui, K. Inui, Y. Kumai, R. Yoshida, D. Suzuki, *ACS Biomater. Sci. Eng*., 2019, **5**, 5615–5622; (e) K. Inui, I. Saito, R. Yoshida, H. Minato, D. Suzuki, *ACS Appl. Polym. Mater.*, 2021, **3**, 3298–3306.

7 (a) T. Ngai, S. H. Behrens, H. Auweter, *Chem. Commun*., 2005, 331–333; (b) S. Fujii, E. S. Read, B. P. Binks, S. P. Armes, *Adv. Mater.*, 2005, **17**, 1014–1018; (c) D. Suzuki, S. Tsuji, H. Kawaguchi, *J. Am. Chem. Soc*., 2007, **129**, 8088–8089; (d) C. Buchcic, R. H. Tromp, M. B. J. Meinders, M. A. C. Stuart, *Soft Matter*, 2017, **13**, 1326–1334; (e) A. Maestro, D. Jones, D. C. S. de Rojas. Candela, E. Guzman, M. H. G. Duits, P. Cicuta, *Langmuir*, 2018, **34**, 7067–7076; (f) D. Wu, V. Mihali, A. Honciuc, *Langmuir*, 2019, **35**, 1, 212–221; (g) T. Watanabe, M. Takizawa, H. Jiang, T. Ngai, D. Suzuki, *Chem. Commun*., 2019, **55**, 5990–5993; (h) Y. Nishizawa, T. Watanabe, T. Noguchi, M. Takizawa, C. Song, K. Murata, H. Minato, D. Suzuki, *Chem. Commun.*, 2022, **58**, 12927–12930.

8 (a) M. Rey, M. A. Fernandez-Rodriguez, M. Karg, L. Isa, N. Vogel, *Acc. Chem. Res.*, 2020, **53**, 414–424; (b). D. Feller, M. Karg, *Soft Matter*, 2022, **18**, 6301–6312.

9 (a) W. Richtering, *Langmuir*, 2012, **28**, 17218–17229; (b) M. A. Fernandez-Rodriguez, A. Martín-Molina, J. Maldonado-Valderrama, *Adv. Colloid Interface Sci.*, 2021, **288**, 102350; (c) S. Stock, R. V. Klitzing, *Curr. Opin. Colloid Interface Sci*., 2022, **58**, 101561.

10 (a) R. H. Pelton, P. Chibante, *Colloids Surf.*, 1986, **20**, 247–256 ; (b) Y. Nishizawa, S. Matsui, K. Urayama, T. Kureha, M. Shibayama, T. Uchihashi, D. Suzuki, *Angew. Chem., Int. Ed*., 2019, **58**, 8809–8813.

11 (a) J. Zhang, R. Pelton, *Langmuir*, 1999, **15**, 8032–8036; (b) H. Minato, M. Murai, T. Watanabe, S. Matsui, M. Takizawa, T. Kureha, D. Suzuki, *Chem. Commun*., 2018, **54**, 932–935.

12 (a) K. Geisel, L. Isa, W. Richtering, *Langmuir*, 2012, **28**, 15770–15776; (b) K. Geisel, K. Henzler, P. Guttmann, W. Richtering, *Langmuir*, 2015, **31**, 83–89; (c) K. Zielińska, H. Sun, R. A. Campbell, A. Zarbakhsh, M. Resmini, *Nanoscale*, 2016, **8**, 4951–4960; (d) M. H. Kwok, T. Ngai, *J. Colloid Interface Sci*., 2016, **461**, 409–418; (e) F. Camerin, M. Á. Fernández-Rodríguez, L. Rovigatti, M. N. Antonopoulou, N. Gnan, A. Ninarello, L. Isa, E. Zaccarelli, *ACS Nano*, 2019, **13**, 4548–4559; (f) R. A. Gumerov, S. A. Filippov, W. Richtering, A. Pich, I. I. Potemkin, *Soft Matter*, 2019, **15,** 3978–3986; (g) J. Harrer, M. Rey, S. Ciarella, H. Löwen, L. M. C. Janssen, N. Vogel, *Langmuir*, 2019, **35**, 32, 10512–10521; (h) Vialetto, S. Ramakrishna, L. Isa, *Sci. Adv*., 2022, **8,** eabq2019

13 (a) K. Horigome, D. Suzuki, *Langmuir*, 2012, **28**, 12962–12970; (b) D. Suzuki, K. Horigome, *J. Phys. Chem. B*, 2013, **117**, 9073–9082; (c) M. Takizawa, Y. Sazuka, K. Horigome, Y. Sakurai, S. Matsui, H. Minato, T. Kureha, D. Suzuki, *Langmuir*, 2018, **34**, 4515–4525; (d) H. Minato, M. Takizawa, S. Hiroshige, D. Suzuki, *Langmuir*, 2019, **35**, 10412–10423; (e) K. Honda, Y. Sazuka, K. Iizuka, S. Matsui, T. Uchihashi, T. Kureha, M. Shibayama, T. Watanabe, D. Suzuki, *Angew. Chem., Int. Ed.*, 2019, **58**, 7294–7298; (f) Y. Sasaki, S. Hiroshige, M. Takizawa, Y. Nishizawa, T. Uchihashi, H. Minato, D. Suzuki, *RSC Adv.*, 2021, **11**, 14562–14567; (g) H. Minato, Y. Sasaki, K. Honda, T. Watanabe, D. Suzuki, *Adv. Mater. Interfaces*, 2022, **9**, 2200879.

14 (a) J. Menath, J. Eatson, R. Brilmayer, A. Andrieu-Brunsen, D. M. A. Buzza, N. Vogel, *Proc. Natl. Acad. Sci.*, 2021, **118**, 52; (b) A. C. Nickel, A. A. Rudov, I. I. Potemkin, J. J. Crassous, W. Richtering, *Langmuir*, 2022, **38**, 4351–4363; (c) J. Vialetto, N. Nussbaum, J. Bergfreund, P. Fischer, L. Isa, *J. Colloid Interface Sci*, 2022, **608**, 2584–2592; (d) K. Kuk, V. Abgarjan, L. Gregel, Y. Zhou, V. C. Fadanelli, I. Buttinoni, M. Karg, *Soft Matter,* 2023, **19**, 175–188.

15 D. Suzuki, *Langmuir*, 2023, **39**, 7525–7529.

16 K. Urayama, T. Saeki, S. Cong, S. Uratani, T. Takigawa, M. Murai, D. Suzuki, *Soft Matter*, 2014, **10**, 9486–9495.

17 (a) X. Wu, R. H. Pelton, A. E. Hamielec, D. R. Woods & W. McPhee, *Colloid Polym. Sci*., 1994, **272**, 467–477; (b) B. R. Saunders, *Langmuir,* 2004, **20**, 3925–3932; (c) M. Stieger, W. Richtering, J. S. Pedersen, P. Lindner, *J. Chem. Phys.*, 2004, **120**, 6197–6206.